Chemical Engineering Journal 430 (2022) 133066

Contents lists available at ScienceDirect

Chemical Engineering Journal

journal homepage: www.elsevier.com/locate/cej

Plasma assisted CO_2 dissociation in pure and gas mixture streams with a ferroelectric packed-bed reactor in ambient conditions

Paula Navascués [a,*], Jose Cotrino [a,b], Agustín R. González-Elipe [a], Ana Gómez-Ramírez [a,b,*]

[a] Laboratory of Nanotechnology on Surfaces and Plasma, Instituto de Ciencia de Materiales de Sevilla (CSIC-Universidad de Sevilla), C/ Américo Vespucio 49, Sevilla 41092, Spain
[b] Departamento de Física Atómica, Molecular y Nuclear, Universidad de Sevilla, Avda. Reina Mercedes, Sevilla 41012, Spain

ARTICLE INFO

Keywords:
Nonthermal plasmas
CO_2 decomposition
Packed-bed reactor
Atmospheric pressure plasma
Ferroelectrics
Optical emission spectroscopy (OES)

ABSTRACT

Carbon dioxide decomposition is a challenging target to combat climate change. Nonthermal plasmas are advantageous for this purpose because they operate at ambient conditions and can be easily scaled-up. In this study, we attempt the CO_2 splitting into CO and O_2 in a parallel plate packed-bed plasma reactor moderated with Lead Zirconate Titanate (PZT) as ferroelectric component, achieving conversion rates and energy efficiencies higher than those obtained with $BaTiO_3$ in our experimental device. The analysis of the reaction mechanisms with optical emission spectroscopy under various operating conditions has shown a direct correlation between energy efficiency and intensity of CO* emission bands. These results and those obtained with a $LiNbO_3$ plate placed onto the active electrode suggest that high temperature electrons contribute to the splitting of CO_2 through an enhancement in the formation of CO_2^+ intermediate species. Results obtained for $CO_2 + O_2$ mixtures confirm this view and suggest that back recombination processes involving CO and O_2 may reduce the overall splitting efficiency. The study of mixtures of CO_2 and dry air has proved the capacity of ferroelectric packed-bed reactors to efficiently decompose CO_2 with no formation of harmful N_XO_Y subproducts in conditions close to those in real facilities. The found enhancement in energy efficiency with respect to that found for the pure gas decomposition supports that new reaction pathways involving nitrogen molecules are contributing to the dissociation reaction. We conclude that PZT moderated packed-bed plasma reactors is an optimum alternative for the decompositon of CO_2 in real gas flows and ambient conditions.

1. Introduction

The growing concern about the continuous increase in carbon dioxide concentration and other greenhouse gases in Earth's atmosphere has fostered the development of new remediation strategies and technologies. One possible way to reverse this situation consists of applying Carbon Capture Storage (CCS) or Utilization (CCU) systems to either hold back or transform CO_2 or other carbon containing harmful gases into valuable products before their release to the atmosphere [1]. Also, carbon dioxide conversion processes have gained much interst for the oxygen production in the CO_2 rich (95%) Mars atmosphere, where promising results have been obtained recently by the Moxie experiment carried out in the red planet applying a high temperature decomposition technique [2].

Current strategies for CO_2 decomposition and/or revalorization face the problem of the high stability of this molecule. From a thermodynamic point of view, either its dissociation breaking or just its activation are highly demanding energetic processes (e.g., C = O doubled bound energy is 783 kJ/mol, while the Gibbs free energy of formation of CO_2 is 394 kJ/mol [3]). The energetic requirements imposed by these internal energy parameters are particularly relevant if the intended process is the splitting of CO_2 into CO and O_2 induced by plasma. Plasma technologies promote this splitting through the excitation of CO_2 molecules by different elemental processes followed by a series of subsequent intermediate reactions ending up in the production of the desired products. In particular, in nonthermal plasmas far from the thermodynamic equilibrium, such as those based on a dielectric barrier discharge (DBD) at atmospheric pressure, mean electron temperatures typically vary between 1 and 10 eV, a wide range enabling the direct activation of the CO_2 molecule by electron impact through either electronic excitation, ionization or dissociation mechanisms [4].

Due to their operational advantages, DBD reactors and packed-bed

* Corresponding authors at: Departamento de Física Atómica, Molecular y Nuclear, Universidad de Sevilla, Avda. Reina Mercedes, Sevilla 41012, Spain.
E-mail addresses: paula.navascues@icmse.csic.es (P. Navascués), anamgr@us.es (A. Gómez-Ramírez).

https://doi.org/10.1016/j.cej.2021.133066
Received 6 August 2021; Received in revised form 12 October 2021; Accepted 13 October 2021
Available online 26 October 2021

systems filled with different materials have been extensively utilized during the last decade to induce various CO_2 conversion or decomposition processes [5-10]. In fact, DBD methods are safe, easily scalable, have relatively low energetic requirements, have short induction times and can be easily coupled to renewable (and intermittent) wind or solar electricity. Additionally, packed-bed reactors can easily incorporate catalytic materials to promote plasma and catalysis synergies. Examples of dielectric materials used to moderate the CO_2 plasma splitting reaction include Al_2O_3, ZrO_2, or SiO_2 beds among others [3,11-13]. In general, energy efficiencies around 5% have been obtained with these conventional dielectrics, with some exceptions like the 12% obtained by Ozkan *et al.*, using power modulation strategies operating in burst mode instead of a conventional AC mode [14,15]. More recently, non-conventional materials such as polyurethane foams or core–shell structures have been also utilized as dielectric bed materials, but reported energy efficiencies of plasma processes only amount to ca. 5% for meaningful splitting rates [16-18].

To overcome such an apparent energy efficiency limit of packed-bed reactors moderated with dielectric materials, ferroelectrics, particularly the most common $BaTiO_3$, and/or catalytically active beds, have been essayed as moderator materials for the CO_2 plasma conversion [6,10,12,19-26]. Using some of these approaches, the CO_2 plasma spliting mechanism has been also extensively studied seeking for procedures favouring the most efficient processes. For example, Xin tu *et al.* have reported that catalyst surfaces with oxygen vacancies can efficiently promote the dissociation of the CO_2 molecule and, based on additional evidences, proposed a decomposition mechanism triggered by the breaking of the C = O bond upon interaction with plasma electrons [19,24,25]. This mechanism differs from that proposed for the CO_2 decomposition induced in microwave (MW) and gliding arc (GA) reactors that, operating at boundary conditions between thermal and nonthermal plasmas (i.e., conditions usually referred as "warm plasmas"), seem to favour a CO_2 decomposition mechanism mediated by the vibrational excitation of the molecule [27-29]. In DBD and packed-bed reactors the average electron temperature uses to be too high to efficiently induce the dissociation through vibrationally excitations, a fact that explains in part the energy efficiency limitations of this technology [4,30].

In the present work, we study the usage of a ferroelectric packed-bed plasma reactor with a parallel plate configuration to induce the decomposition of CO_2 at ambient temperature and atmospheric pressure. As a way to overcome the aforementioned energetic limit, we propose the use of Lead Zirconate Titanate (PZT) as moderator to induce the decomposition of CO_2 into CO and O_2. This ferroelectric material has provided remarkable reaction yields for the synthesis of ammonia in the same reactor and without catalysts [31,32]. The high dielectric permittivity of PZT and its much higher Curie temperature than $BaTiO_3$ (i.e. 120 °C, lower than the actual temperature of common plasma-catalysis processes) have been recently claimed as key factors accounting for the high performance of packed-bed plasma reactors moderated with this material [33].

The motivation of this work is twofold. Firstly, to determine the efficiency of PZT moderated packed-bed reactors for the splitting of CO_2 and, secondly, to advance in the understanding of the basic mechanisms involved in this reaction, either with pure CO_2 or with mixtures of this gas with oxygen (i.e. $CO_2 + O_2$) and dry air (i.e. CO_2 + air). For this purpose, some experiments have been also carried out incorporating a $LiNbO_3$ plate onto the active electrode, a procedure enabling to assess the influence of the average energy of plasma electrons onto the reaction process and intermediate reaction mechanisms. The utilized configuration is similar to that proposed in a previous work where an extra ferroelectric material barrier was used to increase the removal efficiency of pollutants in air [34]. The analysis of the reaction efficiency under different flow rates and electrical excitation conditions has been complemented with the characterization of the plasma species with the optical emission spectroscopy (OES) technique. This analysis has provided useful data to interpret the reaction and electronic excitation mechanisms of the CO_2 molecules. In line with previous works by Zhang and Harvey [20] and Wolf *et al.* [35], we have also studied $CO_2 + O_2$ mixtures and confirm that back-reactions (i.e. the recombination of CO and O_2 into CO_2) can be detrimental for the overall CO_2 decomposition yield. Finally, considering that in most CO_2 industrial procedures this gas appears combined with air, we have studied mixtures of CO_2 with dry air. Snoeckx *et al.* have shown an increased absolute conversion rate for the CO_2 decomposition reaction when igniting a $CO_2 + N_2$ plasma [36]. Our results show an increasing energy efficiency for a mixture with 15% air and, unlike previous results in literature where harmful N_XO_Y compounds were found as by-product of a plasma reaction of nitrogen and CO_2 [10,36], no traces of nitrogen oxides have been found under our working conditions.

2. Materials and methods

2.1. Reactor setup and electrical diagnosis

The packed-bed plasma reactor consisted of a stainless-steel vessel with two parallel plate aluminium electrodes separated by the packing material (see supplementary material S1 for a detailed description of the reactor). The bottom electrode was grounded and the upper electrode was connected to a high voltage amplifier (Trek Inc., Model PD05034), coupled to an AC sinusoidal function generator (Stanford Research Systems, Model DS345). The voltage amplitude was varied between 2 and 5 kV and the frequency was fixed at 1 kHz, if not otherwise stated. The applied voltage was measured by means of a high voltage probe connected to the active electrode, while the current was determined both with a current transformer (Pearson, Current Monitor Model 6585) and a capacitor (2.5 μF) connected to the ground, the latter to directly acquire the charge transferred through the circuit. All electrical signals were recorded by an oscilloscope (Agilent Tech., Model DSO-X 3024A). Applied power was determined from the area of the Lissajous curves, i.e., from the plots of the transferred charge versus the applied voltage. All the experiments were carried out at atmospheric pressure and ambient temperature. A fan was used to cool down the metal walls of the reactor. All measurements were repeated twice to confirm the results. Reported data are an average of the obtained results for each experimental condition.

The packing material situated between the electrodes consisted of pellets of Lead Zirconate Titanate (PZT). The PZT ferroelectric pellets, supplied as powder by APC International Ltd, were sintered in our laboratory following the procedure described in a previous article [7]. Its relative permittivity is around 1900, its Curie Temperature 332 °C and the pellets have a diameter comprised between 2 and 3 mm. For some experiments the upper electrode was covered with a ferroelectric $LiNbO_3$ plate, a procedure previously utilized by us to change the electron energy distribution function (EEDF) in the plasma for a given operational voltage [34]. The ferroelectric plate (Roditi International Corporation Ltd) was one-side polished and has a diameter of 10 cm, a thickness of 0.5 mm, a Curie Temperature of 1210 °C, and a relative permittivity tensor with diagonal-values of $T_{11} = T_{22} = 85.2$ and $T_{33} = 28.7$. See supplementary material S1 for a more detailed description of the reactor and the experimental set-up. Table 1 summarizes the different barrier architectures utilized in this work. To highlight the advantages of using PZT, some comparative experiments have been also done using pellets of $BaTiO_3$ (see characteristics of pellets in Table 1).

All utilized gases (CO_2, O_2, and dry air) were supplied by Air Liquide (Alphagaz). Different CO_2 flow rates were used to study the effect of the residence time (15, 25 and 40 sccm). Gas mixtures of Carbon Dioxide with O_2 and dry air were analyzed for a total flow rate of 25 sccm and CO_2 concentrations varying from 100 to 90% for O_2 mixtures and from 100% to 80% for air mixtures.

Table 1
Experimental configurations and packed-bed characteristics for different ferroelectric components and inter-electrode distances.

Configuration	Pellets diameter	Active electrode covered by the ferroelectric plate	Inter-electrode (metal–metal) distance
PZT	2 – 3 mm	No	5 mm
PZT-D	2 – 3 mm	$LiNbO_3$	5.5 mm*
BT	2 mm	No	5 mm

*Note that when incorporating the $LiNbO_3$ ferroelectric plate, the inter-electrode metal–metal distance is lengthened to compensate the incorporation of the plate and to keep costant the residence time of the gases in the packed bed.

2.2. Conversion rate, reaction efficiency and carbon balance

Reaction products were characterized with a Quadrupole Mass Spectrometer (QMS, Pfeiffer Vacuum, QMG 220 Prisma Plus). The CO_2 conversion rate, $\chi(\%)$, determined following the intensity of the $m/z = 44$ signal, was defined as:

$$CO_2 \text{ Conversion Rate, } \chi(\%) = \frac{\text{Int}^{\,m/z=44}\ (\text{off}) - \text{Int}^{\,m/z=44}\ (\text{on})}{\text{Int}^{\,m/z=44}\ (\text{off})} \cdot 100\ (\%) \quad (1)$$

where Int $^{m/z=44}$ (off) and (on) are the signal intensities associated with the CO_2^+ ion determined by QMS in a stationary state for plasma *off* and *on* conditions, respectively.

For the gas mixtures (i.e. CO_2 plus O_2 or dry air), the conversion rate has to be corrected multiplying the absolute CO_2 conversion rate, $\chi(\%)$, by the dilution factor:

$$\textit{Effective } CO_2 \textit{ Conversion Rate, } \chi_{eff}(\%) = \chi(\%) \cdot \frac{CO_2 \textit{ flow rate } (L/s)}{\textit{Total flow rate } (L/s)} \quad (2)$$

The specific input energy (SIE) is defined as [3]:

$$SIE\ (kJ/L) = Power\ (kW)/Total\ flow\ rate\ (L/s) \quad (3)$$

where the average power is determined by calculating the area of the Lissajous figure recorded in each case. Electrical measurements were taken at the beginning and at the end of each experiment. If not otherwise stated, to vary the power, and thus the SIE, we changed the applied voltage at constant frequency.

Process efficiency is referred to the standard reaction enthalpy using the energy efficiency term, $\zeta(\%)$. To determine $\zeta(\%)$, we relate the CO_2 conversion rate (absolute or effective, this latter utilized for CO_2 mixtures with other gases) with the SIE and the standard enthalpy of the CO_2 dissociation reaction into CO and O_2, ΔH_0 (283 kJ/mol) [3].

$$\textit{Energy Efficiency, } \zeta\ (\%) = \frac{\chi\ (\%) \cdot \Delta H_0\ (kJ/mol)}{SIE\ (kJ/mol)} \quad (4)$$

Although the dissociation of CO_2 into CO and O_2 has been supposed to be the main reaction pathway, other reactions could occur, in particular, carbon deposition on the packing material and/or on the electrode surfaces. To quantify the amount of deposited carbon, a Carbon Balance parameter, C_B (%), has been defined as the ratio between the outlet flows of the formed CO and unreacted CO_2 and the inlet flow of CO_2 initially fed into the reactor:

$$\textit{Carbon Balance, } C_B\ (\%) = \frac{(CO\ \ out + CO_2\ \ out)\ \ (mol)}{CO_2\ \ in\ \ (mol)} \cdot 100 \quad (5)$$

2.3. Optical emission spectroscopy

Plasma optical emission spectra were collected using a collimator that was placed at a lateral window of the reactor, and connected through an optical fiber to a spectrometer (Horiba Ltd, Jobin-Yvon FHR640). The measurements were taken by means of a diffraction grating that has a density of 1201 lines/cm and is centered at 330 nm. The integration time was 0.5 s and the resolution 0.2 nm. Table 2 summarizes the characteristic optical emission bands recorded for a typical CO_2 plasma and their association to the corresponding excited species and electronic transitions according to literature [10,37-42].

3. Results and discussion

3.1. Effect of PZT as packing bed material

Recent results in our laboratory have shown that PZT performs better than $BaTiO_3$ for the ammonia synthesis in an atmospheric pressure plasma process. Bassically, the higher performance and energy efficiency found for PZT was due to a lowering of the breakdown voltage and an enhancement of the electric field through the packed-bed, both features contributing to reduce the power consumption [31,33]. A first issue in the present investigation is to asses whether similar effects occur with PZT for the CO_2 splitting process.

Fig. 1 shows the CO_2 conversion rate and the energy efficiency for the CO_2 splitting process determined as a function of the SIE for the PZT reactor configuration and various gas flow rates (15, 25, and 40 sccm). SIE has been chosen as x-axis variable to properly compare reaction efficiency at different flow rates and configurations. SIE was changed varying the power for a given flow rate while increasing the applied voltage between 2.5 and 4 kV. The frequency was maintained constant at 1 kHz. The plots in Fig. 1 clearly show an increase in conversion rate and a sharp drop in energy efficiency for increasing values of SIE. This behaviour is common in plasma-driven CO_2 decomposition processes operated in AC mode [6,18,19,43-45] and agrees with results obtained by numerical modelling [46].

Another interesting finding evidenced by the plot in Fig. 1(a) is that the conversion rate, χ (%), increases with the gas flow (or analogously when the residence time decreases). This behaviour differs from that found by other authors that usually report maximum conversion rates for lower CO_2 flows (i.e., for higher resident times) [11,13,44]. We tentatively attribute this difference to the occurrence of back-reactions taken place on the pellets surfaces and/or in the plasma bulk (e.g., $CO + O \rightarrow CO_2$), as it has been claimed by some authors for the CO_2 plasma splitting at high pressures and different reactor configurations [17,35]. From the plots in Fig. 1(a) it is also remarkable that conversion curves almost converge into a single trend for flow rates higher than 25 sccm. Conversely, the fact that the energy efficiency decreases with the SIE and for lower gas flow rates (higher resident time) (c.f. Fig. 1(b)) further supports that back-reactions migh be involved and may detrimentally affect the process efficiency.

Results plotted in Fig. 1 show that, for the PZT configuration, a

Table 2
Emission bands for pure CO_2 plasmas taken from [38-41].

System	Transition	λ (nm)
CO_2^+ (B)	$B^2\Sigma^+ \rightarrow X^2\Pi$	288.3 – 289.6
CO_2^+ (A): Fox, Duffendack and Barker's (FDB) System [1]	$A^2\Pi \rightarrow X^2\Pi$	304.8, 324.6, 313.9, 337.0, 337.7, 355.1, 356.5, 362.1, 369.1, 383.8, 387.0, 396.0, 412.0, 413.7
Third Positive System of CO	$b^3\Sigma^+ \rightarrow a^3\Pi$	283.3, 297.7, 313.4, 330.5, 349.3, 369.9

[1] For the Fox, Duffendack and Barker's System, only high intensity bands are shown (i.e., bands whose intensity is higher than 0.6 in a scale normalized to the most intense line)

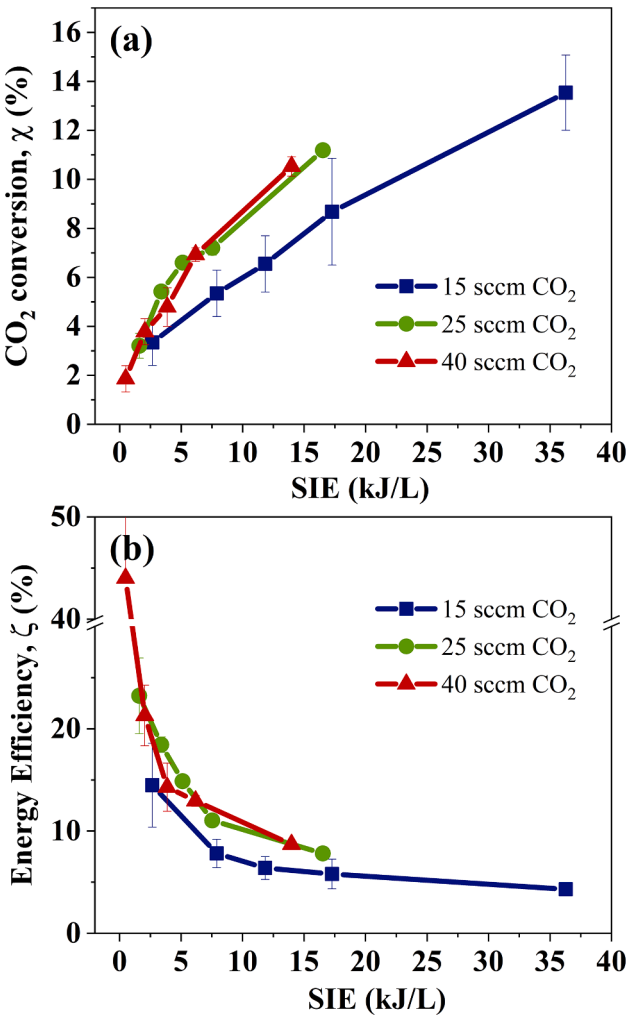

Fig. 1. (a) CO_2 conversion rate and (b) energy efficiency represented versus the SIE values. Experiments were carried out for CO_2 flow rates of 15, 25, and 40 sccm, a frequency of 1 kHz, and voltage amplitude varying between 2.5 and 4.0 kV for the PZT configuration.

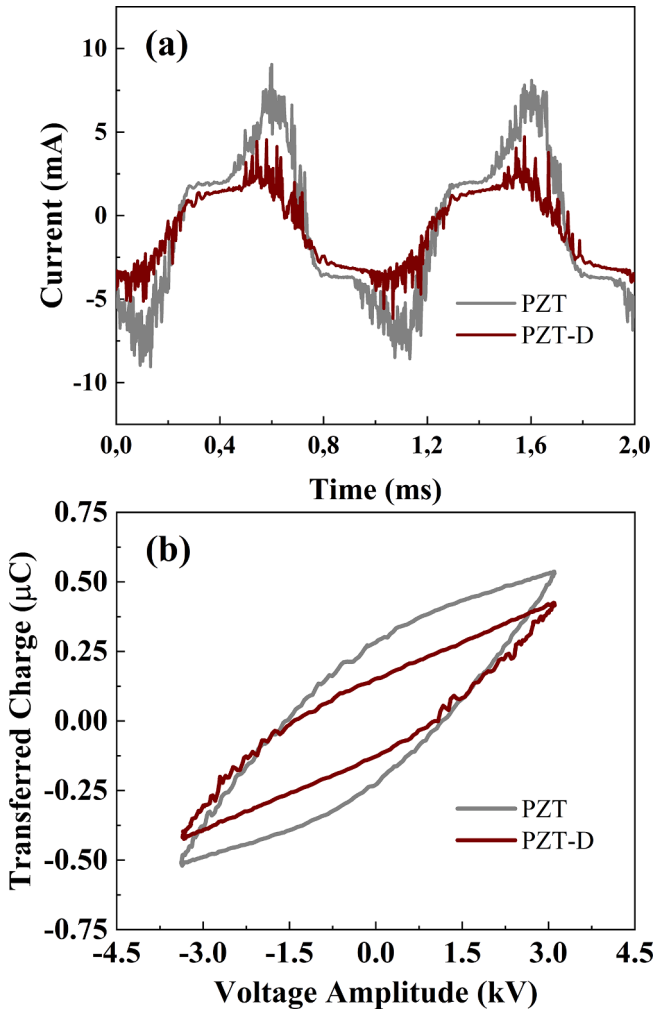

Fig. 2. (a) Measured current and (b) Lissajous curves determined for the indicated experimental configurations (see Table 1) for a CO_2 flow rate of 25 sccm, an applied voltage of 4.0 kV, and a frequency of 1 kHz.

conversion rate of 11% and an energy efficiency of 10% were reached for a SIE of 17 kJ/L, which represents a good trade-off between these two magnitudes. Remarkably, these energy efficiencies were obtained with PZT as packing material, in the absence of a carrier gas or another catalytic material. The corresponding I(t) curves plotted in Fig. 2(a) show that, in agreement with other authors under similar working conditions [14,43], the plasma contains a significantly high amount of microdischarges.

3.2. *Some insights into the reaction mechanisms*

Fig. 3 shows the optical emission spectrum recorded for the reactor in the PZT configuration, an applied voltage of 3.25 kV, a frequency of 3 kHz, and a CO_2 flow rate of 25 sccm. The assignment of the recorded bands, gathered in Table 2, confirms the presence in the plasma of CO* and CO_2^+* excited species. Following this assignment, the third Positive System of CO and the FDB System of CO_2^+ (i.e., CO_2^+(A)) are marked with different solid lines in the figure (black and blue respectively), while the dobble band located between 288 and 290 nm, attributed to CO_2^+(B) emissions, is marked with a dashed line. Differentiating the 288.3 nm and 289.6 nm bands associated to CO_2^+(B) was not possible because of their small intensity and the low spectral resolution available in the packed-bed reactor, where only the light coming from the free space between the pellets contributes to the spectrum.

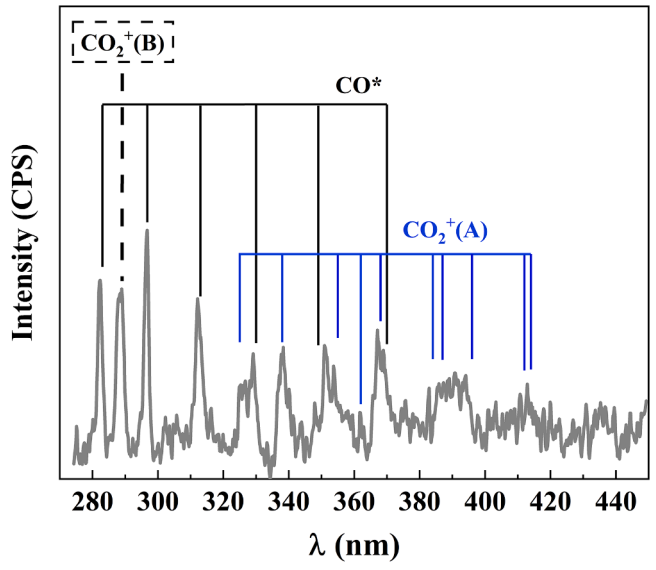

Fig. 3. Characteristic emission spectrum obtained for the PZT configuration, an applied voltage of 3.25 kV, a frequency of 3 kHz, and a CO_2 flow rate of 25 sccm. Bands are assigned according to Table 2.

According to the review by Snoeckx and Bogaerts on CO_2 excitation under DBD conditions (for a reduced electric field higher than 200 Td), the partition of the available electron energy between electronic excitations, dissociation, ionization, and vibrational excitations processes is 70–80%, 5%, 5%, and 10%, respectively [3]. Ferroelectric packed-bed plasmas are characterized by a EEDF that extends to rather high energies (see supplementary material, Figure S2 (c)). In these conditions, even if both surface reactions involving excited species [47] and CO_2 vibrational excitation might contribute to the dissociation reaction (e.g., as in MW plasmas [27,29,48]), it is likely that electron impact dissociation induced by electronic excitation is the dominant mechanism for the CO_2 splitting reaction. The detection in the plasma of both the CO_2^+(B) band between 288 and 290 nm and the CO_2^+(A) FDB emission system supports this assumption (CO_2^+ formation from CO_2 requires ionization energies around 18 eV [40]). In addition, the recording of the characteristic finger print bands of CO* species in our experiment with a relative intensity much higher than in spectra recorded by other authors [10,37,42]), also supports the involvement of high energy electrons. In literature there is not agreement about the spectral characteristics and formation routes of CO* species in CO_2 plasmas. For example, Brehmer *et al.* proposed that the detection of CO* emission bands is the result of reaction intermediates directly leading to the formation of CO in an excited electronic state [37]. Conversely, Du *et al.* proposed that CO is initially formed in its ground state and subsequentially excited through electron impact processes [49]. In the PZT moderated packed-bed reactor, we assume that, in addition to the aforementioned excitation processes of CO_2 proposed in ref. [3], the interaction of CO_2 molecules and CO_2^+ species with high energy electrons efficiently contribute to the CO_2 decompostion through intermediate reactions that lead to the formation of CO* species- :

$$CO_2 + e^-(high\ energy) \rightarrow CO_2^+ \left(CO_2^{+*}\right) + 2e^- \quad (6)$$

$$CO_2 + e^-(high\ energy) \rightarrow CO^* + O + e^- \quad (7)$$

$$CO_2^+ \left(CO_2^{+*}\right) + e^-(high\ energy) \rightarrow CO^* + O \quad (8)$$

where CO_2^+* refers to ionized carbon dioxide molecules in the excited states A or B.

To further support the involvement of high energy electrons in these intermediate reactions we performed two complementary experiments (chemical kinetics modeling would also aid to confirm the occurrence of those reactions). In the first one we used the same 5 mm PZT barrier and placed a $LiNbO_3$ plate directly onto the active electrode (i.e., what is called PZT-D configuration, see Table 1). In a previous work dealing with the removal of air contaminants we proved that the incorporation of a ferroelectric disk in a similar packed-bed ferroelectric reactor served to modify the EEDF, keeping constant the current and increasing the applied voltage [34]. Herein we followed a different strategy, consisting of comparing results for the PZT and PZT-D configurations working at the same voltage which, in the latter case would entail a decrease in the values of the reduced electric field between the pellets. Second experiment consisted of using $BaTiO_3$ instead of PZT as moderator material (BT configuration, see Table 1). A comparative assessment of the CO_2 splitting reaction was therefore carried out with the PZT, PZT-D and BT reactor configurations under similar conditions: a flow rate of 25 sccm, voltage amplitude of 3.25 kV and frequencies of 1, 2, and 3 kHz.

Comparison in Fig. 2(a) of the measured I(t) curves for the PZT and PZT-D configurations shows that microdischarges present a slightly lower intensity in the latter case. This result reflects the increase in system impedance expected because of the incorporation of the $LiNbO_3$ plate. An expected consequence is that, for the same applied voltage, the mean electron energy should be smaller for the PZT-D configuration because the plate will reduce the effective electric field through the barrier of packed bed pellets. These considerations are confirmed by the Lissajous curve in Fig. 2(b) showing a similar but somewhat smaller area for the PZT-D configuration than for the PZT one (note the area of the Lissajous figure is directly related to the consumed power). Electric field distribution and EEDF have been estimated for the two configurations using Comsol Multiphysics [50] and the BOLSIG+ code [51] respectively (see supplementary material S2). These calculations clearly show that the mean electron energy is higher (8.2 eV versus 7.4 eV) and the tail of higher energy electrons larger for the PZT than for the PZT-D configuration.

As expected, conversion rate, energy efficiency and SIE values were smaller for the PZT-D configuration in comparison with the values of these parameteres for the PZT (c.f., Table 3). Very remarkalby, the OES analysis of the plasma also suggested considerable mechanistic differences for these two configurations. Fig. 4 shows a normalized representation of the OES zoomed at the 280–300 nm zone as a function of the SIE/frequency values the three experimental conditions: PZT, PZT-D and BT (a comparison between the complete spectra is reported in the supplementary material S3). Fig. 4 (a) shows that for the PZT configuration, the higher the frequency/SIE value the higher the intensity of the CO* band. This tendency is not observed for the PZT-D configuration. We attribute this difference to that the larger population of high energy electrons in the interpellet space predicted by Comsol/BOLSIG+ for the PZT case efficiently contributes to increase the probability of reactions [7-8] (see supplementary material S2). The relatively higher conversion rate of CO_2 into CO found for the PZT system (see Table 3) also agrees with this assumption (in this case conversion doubled when the frequency was multiplied by a factor of 3, in line with the progressive formation of more CO* plasma species revealed by OES). Conversely, for the PZT-D configuration, the fact that the intensity of the CO* emission bands remains constant (c.f. Fig. 4 (b)) while the conversion rate increases (Table 3) supports that CO* emission is not only related to the CO concentration in the outlet products (i.e., to the CO_2 conversion rate), as proposed in [48], but rather to the population of high energy electrons in the plasma. In other words, we attribute the lower and almost invariable CO* population found for the PZT-D configuration to the lower concentration of energetic electrons in this case (see Comsol and BOLSIG+ simulations in the supplementary material S2 and the experimental results in supplementary material S4, showing that for all applied voltages, the incorporation of the ferroelectric disk rendered lower conversion yields).

Fig. 4(c) and Table 3 show results of the second complementary experiment carried out to prove the importance of high energy electrons for the splitting of CO_2 in ferroelectric packed-bed reactors. In this experiment we used $BaTiO_3$ pellets instead of PZT as packing material. Both conversions and energy efficiencies were lower for the BT than for the PZT reactor configuration (see supplementary material S5). For example, the maximum conversion found for BT and 25 sccm of CO_2 was 9.1 %, with an energy efficiency of 4.5%, results that were worse than those obtained for PZT (see Table 3). These findings correlate with the smaller dielectric constant of $BaTiO_3$ in comparison with PZT at the relatively low working temperatures utilized in this experiment [33] and support the hypothesis that a high dielectric constant contributes to intensify the electric field strength in a packed-bed reactor and to increase the mean electron energy. Recent fluid modelling studies carried out by Van Laer and Bogaerts reported such an effect in the channels of voids between pellets [52,53]. The discharge mode might also depend on the dielectric constant of the pellets. By fluid modeling and iCCD imaging, Wang et al. have demonstrated that the discharge mode may evolve from surface discharges over the whole packing material to a local filamentary mode as the dielectric constant of the material increases [54]. This evolution would also favor the CO_2 splitting process in the PZT moderated packed-bed reactor, because of an increase in the average electron energy in the filamentary mode. The existence of different EEDFs for the BT and PZT reactor condigurations was also supported by the comparion of the OES spectra recorded in each case (c.f., Fig. 4 (a,c) and S3 for the complete spectra). The absence of high intensity bands due to the Third Positive System of CO for the BT case (i.

Table 3
Conversion rate, energy efficiency and SIE values for the reaction carried out with PZT, PZT-D, and BT reactor configurations (see Table 1) at different frequencies, a constant applied voltage of 3.25 kV and a flow rate of 25 sccm CO_2.

f (kHz)	PZT χ(%)	ζ(%)	SIE (kJ/L)	PZT-D χ(%)	ζ(%)	SIE (kJ/L)	BT χ(%)	ζ(%)	SIE (kJ/L)
1	6.6	15	5.1	2.7	11	2.9	1.9	3.6	6.2
2	11	9.7	13	3.8	6.5	3.2	5.8	4.8	14
3	13	6.8	20	4.7	9.3	6.9	9.1	4.5	23

e., a similar behaviour than with the PZT-D configuration) agrees with a lower electric field and, consequently, a lower concentration of high energy electrons in the plasma phase in this case.

3.3. Minority and side-reaction processes

Besides the direct splitting of CO_2 into CO and O, other minority global processes could also take place under our reaction conditions. These include, for example, the direct transformation of CO_2 into carbon and oxygen:

$$CO_2 \rightarrow C + O_2 \quad (9)$$

or the Boudouard reaction:

$$CO \rightarrow CO_2 + C \quad (10)$$

among others [55]. Note that chemical equations (9) and (10) denote global processes that may encompass intermediate reactions taking place in the plasma bulk or onto the surface of the pellets and, therefore involve quite different reactions pathways. Direct evidence of such minority global processes was gained by X-Ray Photoelectron Spectroscopy (XPS) analysis of the packing material before and after plasma exposure (see supplementary material S6). This surface analysis revealed the formation of a carbon deposit, evidenced by a significant increase of the C1s band at 284.6 eV attributed to graphite-like carbon, and a considerable incorporation of carbonate like species, deduced by the deployment of a intense C1s contribution at around 290 eV [56]. A rough estimation from the intensity of the C1s and Ti2p peaks suggests that at least 6 equivalent monolayers of carbonaceous products have been deposited on the surface of ferroelectric pellets utilized for operation periods longer than 20 h (see supplementary material S6).

On the other hand, the analysis of the evolution of carbon balance for the CO_2 splitting reaction indicates that not all the CO_2 entering the reactor gets out in the form of CO or unreacted CO_2. The results reported in the supplementary material S7 show that carbon balance is never 100% and decreases up to values around 85% at higher SIEs. We tentatively relate the occurrence of these alternative splitting reactions with the high energy of electrons existing in the ferroelectric packed-bed reactor filled with PZT. This hypothesis is confirmed by the higher carbon balance always found for the BT and PZT-D configurations, as reported in Figure S7.

3.4. $CO_2 + O_2$ mixtures

Small percentages of oxygen usually appears mixed with CO_2 in, for example, outlet gases from power plants where it is common to find a 5% O_2 after water removal [57]. To analyse the CO_2 splitting process under more realistic conditions, we studied the CO_2 decomposition reaction using mixtures of CO_2 and O_2. From a mechanistic point of view, we must note that O_2 is a product of the CO_2 splitting reaction and a potential source of O atoms and other excited species of oxygen that might contribute to the occurrence of reaction pathways leading to the formation of CO_2. Taking into account the C deposition mentioned in the previous section and the main reaction products (CO and O_2), all those reaction pathways could be included in the following global chemical equations:

$$C + O_2 \rightarrow CO_2 \quad (11)$$

$$CO + O + M \rightarrow CO_2 + M \quad (12)$$

$$O_2 + CO \rightarrow CO_2 + O \quad (13)$$

Where (11) is referred to a global process that considers the interaction between oxygen molecules and the deposited carbon on the pellet surfaces, and processes (12–13) are the most important recombination reactions (at high pressures) considered by Berthelot and Bogaerts for a zero-dimensional chemical kinetics model [58]. The occurrence of these global processes would contribute to decrease the overall CO_2 conversion rate. A deeper chemical kinetics analysis would be necessary for a detailed description of the reaction pathways.

Fig. 5(a) depicts the effective CO_2 conversion rates and energy efficiences obtained for $CO_2 + O_2$ mixtures with the reactor operated in the PZT configuration and the conditions providing optimum results for CO_2 alone (see Fig. 1). Experiments were carried varying the oxygen percentage in the mixture (5, 10%) at a constant flow rate (25 sccm). The voltage amplitude and frequency were 3.25 kV and 3 kHz, conditions that ensured a considerable conversion and a high intensity of the OES spectra. It is noteworthy here that for the $CO_2 + O_2$ mixtures we could not work at constant SIE (that is, constant consumed power) because the measured current changed when oxygen was added to the gas mixture. These changes in the electrical operating conditions suggest that CO_2 conversion rate and SIE values might account for both changes in the reaction mechanisms and in the physical properties of the discharge.

As observed in Fig. 5(a), the effective CO_2 conversion rate decreases from 13% to 8.5% with the addition of 10% O_2. Absolute CO_2 conversion rate (see supplementary material S8) and energy efficiency follow an analogous tendency, the latter parameter decreasing from 6.8% to 3.8%. Similar tendency was obtained by Zhang and Harvey in a cylindrical packed-bed reactor and $BaTiO_3$ as packing material (see also S8 for a more detailed comparative analysis). Nevertheless, the efficiencies found here are higher (5% for 95/5 mixtures - SIE of 17 kJ/L - versus the 2% reported by these authors - SIE of 103.2 kJ/L -) [20].

Fig. 5(b) shows the optical emission spectra recorded for various O_2 containing mixtures. It is apparent that the relative intensity of the CO* species decreases with respect to that of CO_2^+(B) as the proportion of oxygen in the mixture increases. This tendency agrees with the lower CO_2 splitting yield obtained for the mixture and supports that collisional reaction pathways involving oxygen species could contribute to back global processes of the type (11) and likely (12).

In the spectra of Fig. 5(b) it is also noteworthy the detection of a band around 308–309 nm, that can be attributed to OH* species (common emission at 308.9 nm) [41]. This impurity presumably comes from the interaction between O_2 and the pellets, in agreement with the known capacity of PZT to incorporate hydrogen (e.g., as OH^- or in other forms) onto their surface and in its bulk, a phenomenon that has been recently discussed by us in a previous work [59].

3.5. CO_2 + air mixtures

The CO_2 plasma splitting process has been widely studied using mixtures of CO_2 with other gases, usually referred to as “carrier gases”. Data are available for mixtures CO_2 + O_2 [20,60], CO_2 + N_2

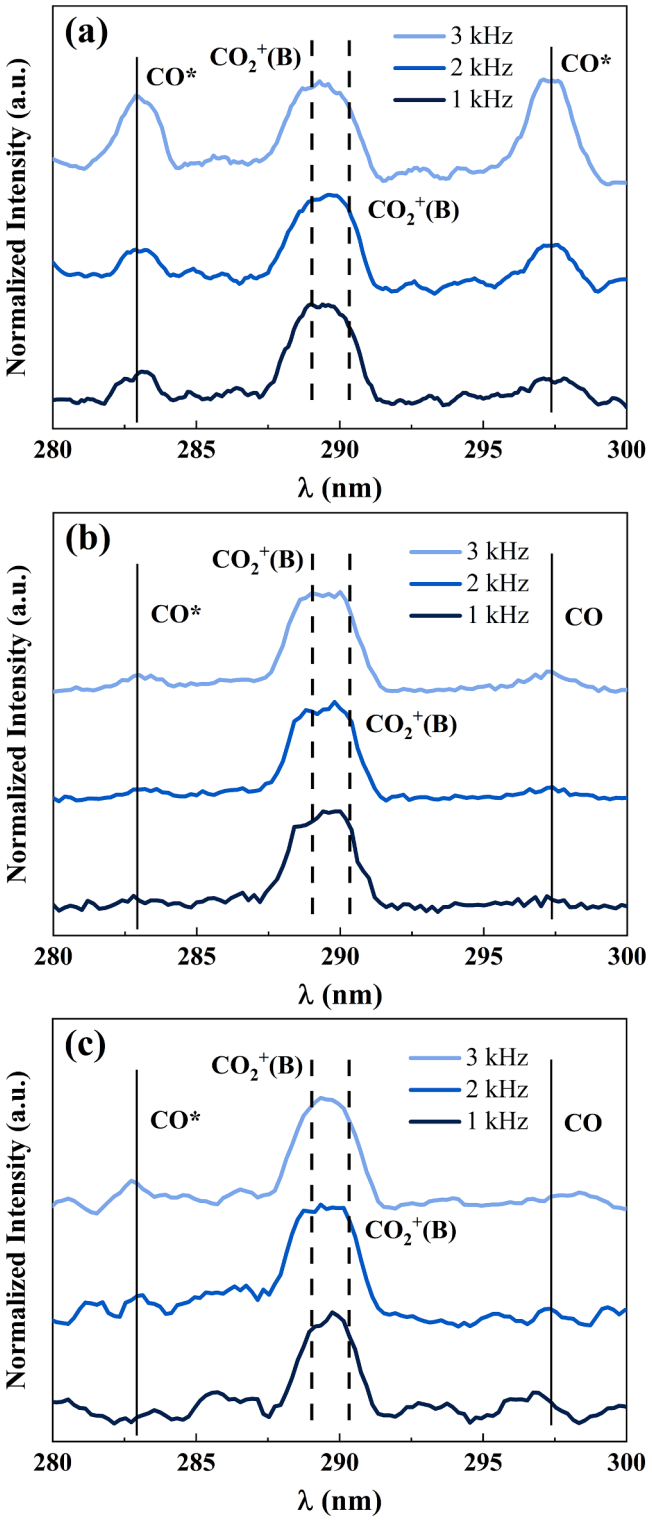

Fig. 4. Optical emission spectra normalized to the intensity of the 288/290 nm band recorded for the (a) PZT, (b) PZT-D, and (c) BT reactor configurations at different frequencies, a constant applied voltage of 3.25 kV and 25 sccm of CO_2.

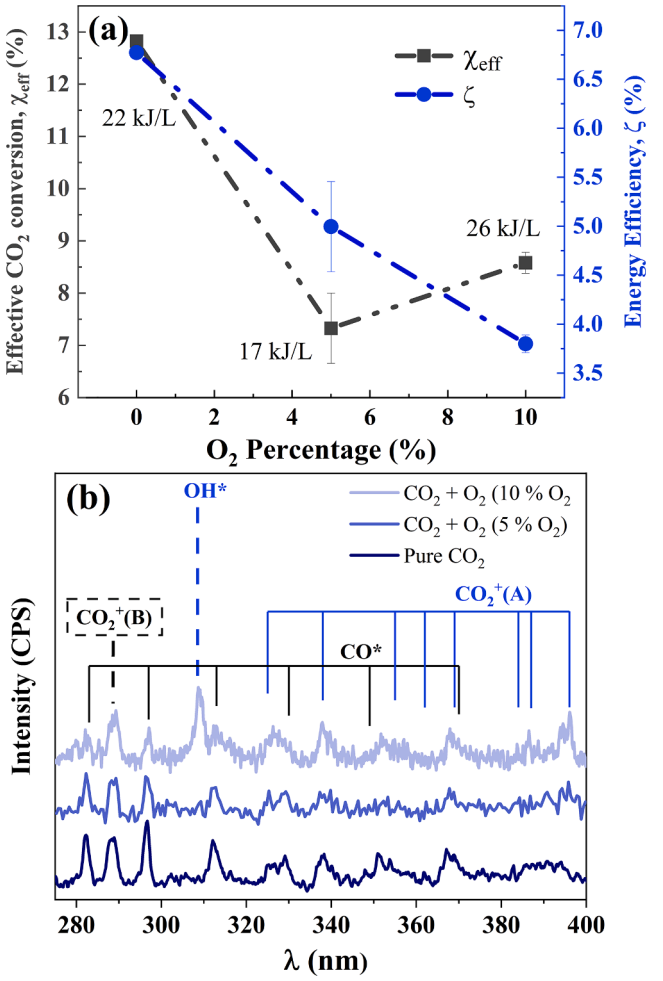

Fig. 5. (a) Effective CO_2 conversion rate and energy efficiency for CO_2 + O_2 mixtures with different O_2 percentages. (b) Associated emission spectra. Experiments were carried out at a frequency of 3 kHz, voltage amplitude of 3.25 kV, and a total flow rate of 25 sccm.

[10,36,61,62], CO_2 + Ar [10,18,61,63] and CO_2 + He [61,63]. However, despite that this is a typical composition of industrial and direct air capture CO_2 outlets, to our knowledge no previous studies have been carried out for mixtures of CO_2 and air in DBD reactors, though a recent study reports the dry reforming of methane adding N_2 and O_2 in a gliding arc reactor [64]. Herein, we have studied the plasma reaction of mixtures of CO_2 with up to 20% dry air (total flow rate of 25 sccm in all cases) at constant voltage amplitude of 3.25 kV and a frequency of 3 kHz. Results are shown in Fig. 6, where both the effective conversion rate and the energy efficiency are plotted as a function of air percentage. Plots show that the effective CO_2 conversion rate changes from 13 to 9.9% when the air percentage varies from 0 to 20%. The energy efficiency increases from 6.8 to 8.1% for the 15% air mixture. Looking at the absolute CO_2 conversion rate (see supplementary material S9), values vary between 7 and 13%. It is important to remark that, as in the case of mixtures with oxygen, SIE was not maintained constant for the experiments (we kept constant the voltage and frequency and let vary the current). Furthermore, from literature it is known that adding small percentages of nitrogen to a CO_2 plasma modifies the electrical behavior of the discharge in a DBD process. Snoeckx *et al.* [36] attribute this change to a transition from a filamentary discharge mode (pure CO_2) to a more homogenous discharge upon N_2 addition. Additionally, these authors studied a wider range of N_2 contents and reported a good agreement between simulation and experimental results [36]. For low nitrogen percentages, similar to those existing in the air mixtures used in this work, they obtain a negligible variation in the energy efficiency of the reaction, concluding that the presence of metastable nitrogen species could influence the reaction mechanisms and compensate the lower CO_2 proportion in the mixture. The authors obtained an energy efficiency of 4.5%, for a mixture of 15% N_2 and a SIE of about 12 kJ/L, while we have reached an efficiency of 8.1% for similar operation conditions. On the

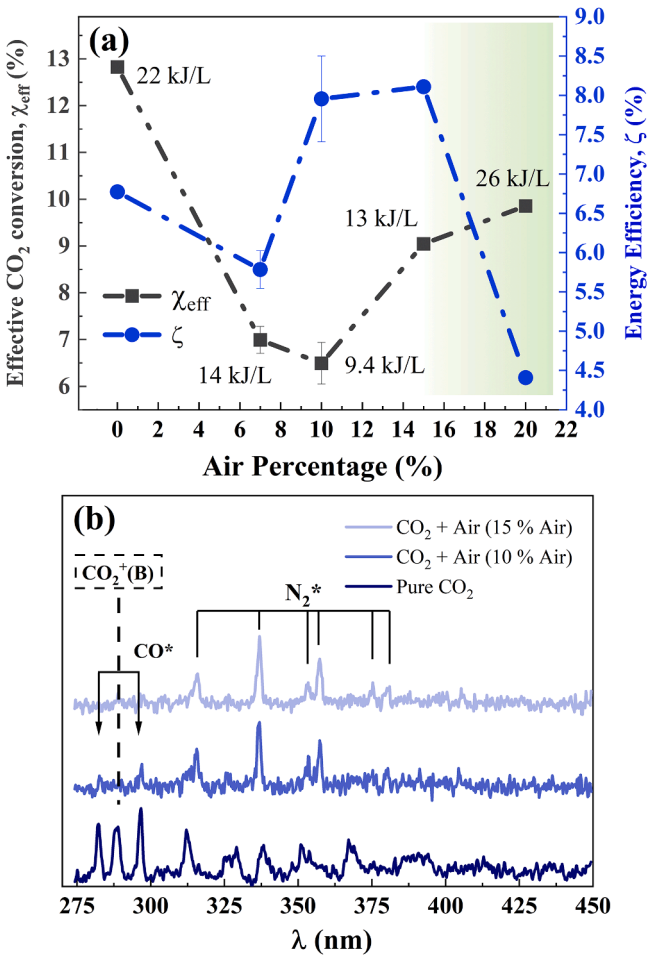

Fig. 6. (a) Effective CO_2 conversion rate and energy efficiency for CO_2 + air mixtures with different air percentages. The SIE values are indicated in the graph. (b) Associated emission spectra. Experiments were carried out for a frequency of 3 kHz, voltage amplitude of 3.25 kV, and a total flow rate of 25 sccm.

other hand, S. Xu *et al.* studied highly diluted N_2 mixtures (from 30% up to 80% of N_2) in a $BaTiO_3$ packed-bed reactor, obtaining that the absolute CO_2 conversion rate increased with the amount of nitrogen in the mixture, though at the expense of a decrease in the energy efficiency [10].

From these studies it is a likely assumption that the noted differences in these articles from literature and our own results could be due both to changes in the reaction mechanism due to the presence of nitrogen molecules and/or to the discharge mode. In our experiment, we assume that the use of PZT as moderator is the main cause of the higher reaction efficiency obtained. Unlike the results in the previous section, showing that the presence of oxygen contributes to diminish conversion and energy efficiency, for the 15% air mixture the combined effect of the major air components - molecular nitrogen and oxygen - results in a reduction of the CO_2 conversion rate and in an increase in energy efficiency by more than 20% with respect the initial value without air. We attribute this behaviour to the occurrence of more efficient reaction pathways involving nitrogen species, as discussed below. For an air percentage of 20% the conversion rate still increases but at expenses of a drastic decrease in the energy efficiency that drops to 4.3% (this reflects the drastic increase in the SIE to 26 kJ/L, because of the increase in the current intensity for this gas mixture). A similar behaviour has been reported for CO_2 + N_2 mixtures and attributed to the increase in the nitrogen concentration in the mixture [36].

Fig. 6(b) shows that the addition of air entirely modifies the plasma emission spectra with respect to those recorded with pure CO_2. The CO* signal significantly decreased for the 10% mixture to disappear with 15% of dry air. Meanwhile no traces CO_2^+(B) emissions could be detected for the mixtures. These bands are replaced by those of the second positive system of N_2* (i.e., [$C^3\Pi \rightarrow B^3\Pi$] transition), with the main band situated at 357.9 nm (note that the spectra did not provided any hint of the formation of the rather common N_2^+ species, usually identified by its first negative system at 391.4 nm). These changes in the OES spectra prove that N_2 from air changes radically the plasma excitation mechanisms and, as a result, the CO_2 splitting pathways. Since the dissociation of the neutral, CO_2, and ionized molecule, CO_2^+, through the intermediate reactions (6-8), as well as excitation mechanisms for CO_2^+(B) and (A) require a substantial energy cost (between 17 and 18 eV) we propose that their occurrence might in part have been replaced by other lower-energy reaction pathways as, for example, the electron impact excitation of N_2 and the formation of other metastable states able to promote an efficient dissociation of CO_2 [36].

An important feature of these experiments with CO_2 + air mixtures is that, unlike previous results for CO_2 + N_2 mixtures in similar reactors [10,36], no N_xO_y species have been detected as reaction by-products (see supplementary material S10), even if no additional reactant is added to the gas mixture (e.g., Snoeckx *et al.* recently published the addition of CH_4 to act as chemical oxygen scavenger to diminish the NO and NO_2 production in CO_2 + N_2 mixtures [65]). We attribute this finding to the specific conditions of the PZT moderated packed-bed reactor and to the ignition of mixtures of CO_2 with air, and not only with N_2. On the one hand, and as stated in the literature, for CO_2 + N_2 plasmas the formation of NO and NO_2 is supposed to proceed via oxygen interaction with nitrogen atoms and electronically excited N_2 molecules [36]. Threshold electron energies required for nitrogen dissociation and excitation by electron impact are 18.5 eV [66] and 7.7 eV [10], respectively. Taking into account these values and the results in Fig. 6 (b), where only the N_2* system is observed upon air addition, we hypothesize that the nitrogen excitation by electron impact is the main process taking place, a fact that could be related to a decrease in the electron temperature (not enough to produce CO_2^{+*} species). On the other hand, the presence of oxygen molecules from the air could affect the chemical reactions, thus hampering the interaction between oxygen and nitrogen atoms to produce N_xO_y species. This assumption agrees with the recent study by Slaets *et al.*, where no traces of N_xO_y species were detected in a gliding arc plasmatron working with methane and carbon dioxide in mixtures containing nitrogen and oxygen [64]. Nevertheless, further computational studies would be needed to unravel the reaction mechanisms occurring in ferroelectric packed-bed configurations.

4. Conclusions

In this work we have studied the CO_2 dissociation process into CO and O_2 in a ferroelectric packed-bed plasma reactor operated at atmospheric pressure and ambient temperature. The obtained results have shown that PZT is an optimum ferroelectric packing material to moderate the plasma discharge in packed-bed reactors, outperforming the more widely used $BaTiO_3$. Its usefulness have been proved not only for the activation of pure CO_2 plasmas, but also for mixtures of CO_2 and air. The high reactor performance achieved with PZT has been attributed to that, at low operation temperatures, its relatively higher dielectric constant contributes to enhance the electric field in the channel of voids between pellets, where high energetic electrons will trigger a series of intermediate reactions contributing to the overall reaction yield.

Analyzing the effect of the barrier architecture (PZT vs. PZT-D configurations, see Table 1) and the CO_2 flow rate (15, 25 and 40 sccm), it is found that best results are obtained with the PZT configuration and high CO_2 flow rates, i.e., for relatively shorter residence time of reactants in the reactor. Moreover, the thorough OES characterization of the plasma carried out in this work for various experimental conditions and the

lower reaction performance obtained when adding a ferroelectric plate to the barrier architecture has been justified because of changes in the EEDF and a decrease in the average energy of plasma electrons in this latter case. We conclude that high energy electrons generated in the discharge moderated with PZT are decisive to produce CO* species and to improve the overall reaction efficiency.

The incidence of back-reactions in diminishing the process efficiency has been scarcely studied experimentally. Our experiments with CO_2 + O_2 mixtures have shown that reactions between excited species of oxygen and CO in the plasma bulk may occur under our working conditions and contribute to the observed decrease in the CO_2 conversion rate when using low flow rates. In this regard, the higher energy efficiency obtained when igniting pure CO_2 plasma at higher flow rates, i.e. for lower residence times, is a result that further supports the occurrence of back-reactions. It is also possible that these back or recombination reactions take place on the surface of the pellets, involving the carbonaceous residues proved by XPS and suggested by the carbon balance analysis.

Finally, a remarkable result of this investigation is that CO_2 decomposition was rather efficient when using CO_2 + air mixtures, reproducing common conditions in real facilities. The good trade-off between conversion rate (9%) and energy efficiency (8.1%) obtained for a 15% air mixture has been accounted for by the involvement of excited nitrogen species in alternative energetically favourable CO_2 decomposition processes. The absence of any N_XO_Y as reaction byproducts is another remarkable result that proves the suitability of packed-bed plasma reactors moderated with PZT for CO_2 splitting at ambient conditions and mixtures with air.

Declaration of Competing Interest

The authors declare that they have no known competing financial interests or personal relationships that could have appeared to influence the work reported in this paper

Acknowledgements

This research was supported by the AEI-MICINN (Project PID2020-114270RA-I00 and PID2020-112620 GB-I00) and by the Consejería de Economía y Conocimiento de la Junta de Andalucía (PAIDI-2020 through project P18-RT-3480 and FEDER-US-1380977).

Appendix A. Supplementary data

Supplementary data to this article can be found online at https://doi.org/10.1016/j.cej.2021.133066.

References

[1] R.M. Cuéllar-Franca, A. Azapagic, Carbon capture, storage and utilisation technologies: A critical analysis and comparison of their life cycle environmental impacts, J. CO2 Util. 9 (2015) 82–102, https://doi.org/10.1016/j.jcou.2014.12.001.

[2] MOXIE for Scientists - NASA Mars, (n.d.). https://mars.nasa.gov/mars2020/spacecraft/instruments/moxie/for-scientists/ (accessed June 16, 2021).

[3] R. Snoeckx, A. Bogaerts, Plasma technology-a novel solution for CO_2 conversion? Chem. Soc. Rev. 46 (19) (2017) 5805–5863, https://doi.org/10.1039/C6CS00066E.

[4] A. George, B. Shen, M. Craven, Y. Wang, D. Kang, C. Wu, X. Tu, A review of non-thermal plasma technology: a novel solution for CO_2 conversion and utilization, Renew. Sustain. Energy Rev. 135 (2021) 109702, https://doi.org/10.1016/j.rser.2020.109702.

[5] M. Mikhail, P. Da Costa, J. Amouroux, S. Cavadias, M. Tatoulian, S. Ognier, M. E. Gálvez, Electrocatalytic behaviour of CeZrO: x-supported Ni catalysts in plasma assisted CO_2 methanation, Catal. Sci. Technol. 10 (14) (2020) 4532–4543, https://doi.org/10.1039/D0CY00312C.

[6] D. Mei, X. Zhu, Y.-L. He, J.D. Yan, X. Tu, Plasma-assisted conversion of CO_2 in a dielectric barrier discharge reactor: Understanding the effect of packing materials, Plasma Sources Sci. Technol. 24 (1) (2015) 015011, https://doi.org/10.1088/0963-0252/24/1/015011.

[7] A.M. Montoro-Damas, J.J. Brey, M.A. Rodríguez, A.R. González-Elipe, J. Cotrino, Plasma reforming of methane in a tunable ferroelectric packed-bed dielectric barrier discharge reactor, J. Power Sources 296 (2015) 268–275, https://doi.org/10.1016/j.jpowsour.2015.07.038.

[8] A. Gómez-Ramírez, V.J. Rico, J. Cotrino, A.R. González-Elipe, R.M. Lambert, Low temperature production of formaldehyde from carbon dioxide and ethane by plasma-assisted catalysis in a ferroelectrically moderated dielectric barrier discharge reactor, ACS Catal. 4 (2) (2014) 402–408, https://doi.org/10.1021/cs4008528.

[9] R. Michiels, Y. Engelmann, A. Bogaerts, Plasma catalysis for CO_2 hydrogenation: unlocking new pathways toward CH_3OH, J. Phys. Chem. C 124 (47) (2020) 25859–25872, https://doi.org/10.1021/acs.jpcc.0c07632.

[10] S. Xu, J.C. Whitehead, P.A. Martin, CO_2 conversion in a non-thermal, barium titanate packed bed plasma reactor: the effect of dilution by Ar and N_2, Chem. Eng. J. 327 (2017) 764–773, https://doi.org/10.1016/j.cej.2017.06.090.

[11] Y. Uytdenhouwen, S. van Alphen, I. Michielsen, V. Meynen, P. Cool, A. Bogaerts, A packed-bed DBD micro plasma reactor for CO_2 dissociation: does size matter? Chem. Eng. J. 348 (2018) 557–568, https://doi.org/10.1016/j.cej.2018.04.210.

[12] I. Michielsen, Y. Uytdenhouwen, J. Pype, B. Michielsen, J. Mertens, F. Reniers, V. Meynen, A. Bogaerts, CO_2 dissociation in a packed bed DBD reactor: first steps towards a better understanding of plasma catalysis, Chem. Eng. J. 326 (2017) 477–488, https://doi.org/10.1016/j.cej.2017.05.177.

[13] K. VanLaer, A. Bogaerts, Improving the conversion and energy efficiency of carbon dioxide splitting in a zirconia-packed dielectric barrier discharge reactor, Energy Technology. 3 (10) (2015) 1038–1044, https://doi.org/10.1002/ente.201500127.

[14] A. Ozkan, A. Bogaerts, F. Reniers, Routes to increase the conversion and the energy efficiency in the splitting of CO_2 by a dielectric barrier discharge, J. Phys. D Appl. Phys. 50 (8) (2017) 084004, https://doi.org/10.1088/1361-6463/aa562c.

[15] A. Ozkan, T. Dufour, T. Silva, N. Britun, R. Snyders, A. Bogaerts, F. Reniers, The influence of power and frequency on the filamentary behavior of a flowing DBD - application to the splitting of CO_2, Plasma Sources Sci. Technol. 25 (2) (2016) 025013, https://doi.org/10.1088/0963-0252/25/2/025013.

[16] Y. Uytdenhouwen, V. Meynen, P. Cool, A. Bogaerts, The potential use of core-shell structured spheres in a packed-bed DBD plasma reactor for CO_2 conversion, Catalysts. 10 (5) (2020) 530, https://doi.org/10.3390/catal10050530.

[17] P. Kaliyappan, A. Paulus, J. D'Haen, P. Samyn, Y. Uytdenhouwen, N. Hafezkhiabani, A. Bogaerts, V. Meynen, K. Elen, A.n. Hardy, M.K. Van Bael, Probing the impact of material properties of core-shell SiO2@TiO2spheres on the plasma-catalytic CO_2 dissociation using a packed bed DBD plasma reactor, J. CO2 Util. 46 (2021) 101468, https://doi.org/10.1016/j.jcou.2021.101468.

[18] H. Taghvaei, E. Pirzadeh, M. Jahanbakhsh, O. Khalifeh, M.R. Rahimpour, Polyurethane foam: a novel support for metal oxide packing used in the non-thermal plasma decomposition of CO_2, J. CO2 Util. 44 (2021) 101398, https://doi.org/10.1016/j.jcou.2020.101398.

[19] D. Mei, X. Zhu, C. Wu, B. Ashford, P.T. Williams, X. Tu, Plasma-photocatalytic conversion of CO_2 at low temperatures: understanding the synergistic effect of plasma-catalysis, Appl. Catal. B 182 (2016) 525–532, https://doi.org/10.1016/j.apcatb.2015.09.052.

[20] K. Zhang, A.P. Harvey, CO_2 decomposition to CO in the presence of up to 50% O_2 using a non-thermal plasma at atmospheric temperature and pressure, Chem. Eng. J. 405 (2021) 126625, https://doi.org/10.1016/j.cej.2020.126625.

[21] T. Butterworth, R. Elder, R. Allen, Effects of particle size on CO_2 reduction and discharge characteristics in a packed bed plasma reactor, Chem. Eng. J. 293 (2016) 55–67, https://doi.org/10.1016/j.cej.2016.02.047.

[22] K. Zhang, G. Zhang, X. Liu, A.N. Phan, K. Luo, A study on co_2 decomposition to CO and O_2 by the combination of catalysis and dielectric-barrier discharges at low temperatures and ambient pressure, Ind. Eng. Chem. Res. 56 (12) (2017) 3204–3216, https://doi.org/10.1021/acs.iecr.6b04570.

[23] N.A. Lu, N. Liu, C. Zhang, Y. Su, K. Shang, N. Jiang, J. Li, Y. Wu, CO_2 conversion promoted by potassium intercalated g-C_3N_4 catalyst in DBD plasma system, Chem. Eng. J. 417 (2021) 129283, https://doi.org/10.1016/j.cej.2021.129283.

[24] L.I. Wang, X. Du, Y. Yi, H. Wang, M. Gul, Y. Zhu, X. Tu, Plasma-enhanced direct conversion of CO_2 to CO over oxygen-deficient Mo-doped CeO_2, Chem. Commun. 56 (94) (2020) 14801–14804, https://doi.org/10.1039/D0CC06514E.

[25] B. Ashford, Y. Wang, C.-K. Poh, L. Chen, X. Tu, Plasma-catalytic conversion of CO_2 to CO over binary metal oxide catalysts at low temperatures, Appl. Catal. B 276 (2020) 119110, https://doi.org/10.1016/j.apcatb.2020.119110.

[26] S. Xu, P.I. Khalaf, P.A. Martin, J.C. Whitehead, CO_2 dissociation in a packed-bed plasma reactor: effects of operating conditions, Plasma Sources Sci. Technol. 27 (7) (2018) 075009, https://doi.org/10.1088/1361-6595/aacd6a.

[27] N. Britun, T. Silva, G. Chen, T. Godfroid, J. van der Mullen, R. Snyders, Plasma-assisted CO_2 conversion: Optimizing performance via microwave power modulation, J. Phys. D Appl. Phys. 51 (14) (2018) 144002, https://doi.org/10.1088/1361-6463/aab1ad.

[28] M. Ramakers, G. Trenchev, S. Heijkers, W. Wang, A. Bogaerts, Gliding arc plasmatron: providing an alternative method for carbon dioxide conversion, ChemSusChem 10 (12) (2017) 2642–2652, https://doi.org/10.1002/cssc.201700589.

[29] N. den Harder, D.C.M. van den Bekerom, R.S. Al, M.F. Graswinckel, J. M. Palomares, F.J.J. Peeters, S. Ponduri, T. Minea, W.A. Bongers, M.C.M. van de Sanden, G.J. van Rooij, Homogeneous CO_2 conversion by microwave plasma: wave propagation and diagnostics, Plasma Processes Polym. 14 (2017) 1600120, https://doi.org/10.1002/ppap.201600120.

[30] V. Vermeiren, A. Bogaerts, Improving the energy efficiency of CO_2 conversion in nonequilibrium plasmas through pulsing, J. Phys. Chem. C 123 (29) (2019) 17650–17665, https://doi.org/10.1021/acs.jpcc.9b02362.

[31] A. Gómez-Ramírez, J. Cotrino, R.M. Lambert, A.R. González-Elipe, Efficient synthesis of ammonia from N_2 and H_2 alone in a ferroelectric packed-bed DBD

reactor, Plasma Sources Sci. Technol. 24 (6) (2015) 065011, https://doi.org/10.1088/0963-0252/24/6/065011.
[32] A. Gómez-Ramírez, A.M. Montoro-Damas, J. Cotrino, R.M. Lambert, A.R. González-Elipe, About the enhancement of chemical yield during the atmospheric plasma synthesis of ammonia in a ferroelectric packed bed reactor, Plasma Processes Polym. 14 (2017), https://doi.org/10.1002/ppap.201600081.
[33] A. Gómez-Ramírez, R. Álvarez, P. Navascués, F.J. García-García, A. Palmero, J. Cotrino, A.R. González-Elipe, Electrical and reaction performances of packed-bed plasma reactors moderated with ferroelectric or dielectric materials, Plasma Processes Polym. 18 (3) (2021) 2000193, https://doi.org/10.1002/ppap.202000193.
[34] A. Gómez-Ramírez, A. Montoro-Damas, M.A. Rodríguez, A. González-Elipe, J. Cotrino, Improving the pollutant removal efficiency of packed-bed plasma reactors incorporating ferroelectric components, Chem. Eng. J. 314 (2017) 311–319, https://doi.org/10.1016/j.cej.2016.11.065.
[35] A.J. Wolf, F.J.J. Peeters, P.W.C. Groen, W.A. Bongers, M.C.M. van de Sanden, CO_2 Conversion in nonuniform discharges: disentangling dissociation and recombination mechanisms, J. Phys. Chem. C 124 (31) (2020) 16806–16819, https://doi.org/10.1021/acs.jpcc.0c03637.
[36] R. Snoeckx, S. Heijkers, K. Van Wesenbeeck, S. Lenaerts, A. Bogaerts, CO_2 conversion in a dielectric barrier discharge plasma: N_2 in the mix as a helping hand or problematic impurity? Energy Environ. Sci. 9 (3) (2016) 999–1011, https://doi.org/10.1039/C5EE03304G.
[37] F. Brehmer, S. Welzel, M.C.M. van de Sanden, R. Engeln, CO and byproduct formation during CO_2 reduction in dielectric barrier discharges, J. Appl. Phys. 116 (12) (2014) 123303, https://doi.org/10.1063/1.4896132.
[38] G.W. Fox, O.S. Duffendack, E.F. Barker, The spectrum of CO_2, Proc. Natl. Acad. Sci. 13 (5) (1927) 302–307, https://doi.org/10.1073/pnas.13.5.302.
[39] H. Anton, Zur lumineszenz einiger molekülgase bei anregung durch schnelle elektronen II, Annalen Der Physik. 473 (3–4) (1966) 178–193, https://doi.org/10.1002/andp.19654710104.
[40] M.A. Johnson, R.N. Zare, J. Rostas, S. Leach, Resolution of the $\bar{A}/\bar{B}$ photoionization branching ratio paradox for the $^{12}CO_2$+$\bar{B}$(000) state, J. Chem. Phys. 80 (1983) 2407–2428, https://doi.org/10.1063/1.446991.
[41] R.W.B. Pearse, A.G. Gaydon, The Identification of Molecular Spectra, 3rd ed., Chapman & Hall, London, 1965.
[42] N.A. Lu, C. Zhang, K. Shang, N. Jiang, J. Li, Y. Wu, Dielectric barrier discharge plasma assisted CO_2 conversion: understanding the effects of reactor design and operating parameters, J. Phys. D Appl. Phys. 52 (22) (2019) 224003, https://doi.org/10.1088/1361-6463/ab0ebb.
[43] D. Mei, X. Tu, Conversion of CO_2 in a cylindrical dielectric barrier discharge reactor: effects of plasma processing parameters and reactor design, J. CO2 Util. 19 (2017) 68–78, https://doi.org/10.1016/j.jcou.2017.02.015.
[44] Y. Uytdenhouwen, K.M. Bal, I. Michielsen, E.C. Neyts, V. Meynen, P. Cool, A. Bogaerts, How process parameters and packing materials tune chemical equilibrium and kinetics in plasma-based CO_2 conversion, Chem. Eng. J. 372 (2019) 1253–1264, https://doi.org/10.1016/j.cej.2019.05.008.
[45] G. Niu, Y. Qin, W. Li, Y. Duan, Investigation of CO_2 splitting process under atmospheric pressure using multi-electrode cylindrical dbd plasma reactor, Plasma Chem. Plasma Process. 39 (4) (2019) 809–824, https://doi.org/10.1007/s11090-019-09955-y.
[46] S. Ponduri, M.M. Becker, S. Welzel, M.C.M. van de Sanden, D. Loffhagen, R. Engeln, Fluid modelling of CO_2 dissociation in a dielectric barrier discharge, J. Appl. Phys. 119 (9) (2016) 093301, https://doi.org/10.1063/1.4941530.
[47] H.H. Kim, A.A. Abdelaziz, Y. Teramoto, T. Nozaki, K. Hensel, Y.S. Mok, S. Saud, D. B. Nguyen, D.H. Lee, W.S. Kang, Interim report of plasma catalysis: Footprints in the past and blueprints for the future, Inter. J. Plasma Environ. Sci. Technol. 15 (2021), https://doi.org/10.34343/ijpest.2021.15.e01004.
[48] T. Silva, N. Britun, T. Godfroid, R. Snyders, Understanding CO_2 decomposition in microwave plasma by means of optical diagnostics, Plasma Processes Polym. 14 (2017) 1600103, https://doi.org/10.1002/ppap.201600103.
[49] Y. Du, K. Tamura, S. Moore, Z. Peng, T. Nozaki, P.J. Bruggeman, CO ($B1\Sigma^+ \rightarrow A1\Pi$) Angstrom system for gas temperature measurements in CO_2 containing plasmas, Plasma Chem. Plasma Process. 37 (1) (2017) 29–41, https://doi.org/10.1007/s11090-016-9759-5.
[50] COMSOL Multiphysics v.5.5. www.comsol.com , (2019).
[51] G.J.M. Hagelaar, L.C. Pitchford, Solving the boltzmann equation to obtain electron transport coefficients and rate coefficients for fluid models, Plasma Sources Sci. Technol. 14 (4) (2005) 722–733, https://doi.org/10.1088/0963-0252/14/4/011.
[52] K. Van Laer, A. Bogaerts, Fluid modelling of a packed bed dielectric barrier discharge plasma reactor, Plasma Sources Sci. Technol. 25 (1) (2016) 015002, https://doi.org/10.1088/0963-0252/25/1/015002.
[53] K. Van Laer, A. Bogaerts, How bead size and dielectric constant affect the plasma behaviour in a packed bed plasma reactor: a modelling study, Plasma Sources Sci. Technol. 26 (8) (2017) 085007, https://doi.org/10.1088/1361-6595/aa7c59.
[54] W. Wang, H.H. Kim, K. van Laer, A. Bogaerts, Streamer propagation in a packed bed plasma reactor for plasma catalysis applications, Chem. Eng. J. 334 (2018) 2467–2479, https://doi.org/10.1016/J.CEJ.2017.11.139.
[55] D. Ray, P. Chawdhury, K.V.S.S. Bhargavi, S. Thatikonda, N. Lingaiah, C. h. Subrahmanyam, Ni and Cu oxide supported γ-Al_2O_3 packed DBD plasma reactor for CO_2 activation, J. CO2 Util. 44 (2021) 101400, https://doi.org/10.1016/j.jcou.2020.101400.
[56] C.D. Wagner, W.M. Riggs, L.E. Davis, J.F. Moulder, Handbook of X-Ray Photoelectron Spectroscopy, Perkin-Elmer Corporation, Eden Prairie, 1979.
[57] X. Xu, C. Song, R. Wincek, J.M. Andresen, B.G. Miller, A.W. Scaroni, Separation of CO_2 from Power Plant Flue Gas Using a Novel CO_2 "Molecular Basket" Adsorbent, in: ACS Division of Fuel Chemistry, Preprints, 2003: pp. 162–163.
[58] A. Berthelot, A. Bogaerts, Modeling of CO_2 splitting in a microwave plasma: how to improve the conversion and energy efficiency, J. Phys. Chem. C 121 (15) (2017) 8236–8251, https://doi.org/10.1021/acs.jpcc.6b12840.
[59] P. Navascués, J.M. Obrero-Pérez, J. Cotrino, A.R. González-Elipe, A. Gómez-Ramírez, Unraveling discharge and surface mechanisms in plasma-assisted ammonia reactions, ACS Sustainable Chem. Eng. 8 (39) (2020) 14855–14866, https://doi.org/10.1021/acssuschemeng.0c04461.
[60] T. Mikoviny, M. Kocan, S. Matejcik, N.J. Mason, J.D. Skalny, Experimental study of negative corona discharge in pure carbon dioxide and its mixtures with oxygen, J. Phys. D Appl. Phys. 37 (1) (2004) 64–73, https://doi.org/10.1088/0022-3727/37/1/011.
[61] D. Ray, R. Saha, C. Subrahmanyam, DBD plasma assisted CO_2 decomposition: Influence of diluent gases, Catalysts. 7 (2017) 244, https://doi.org/10.3390/catal7090244.
[62] L. Terraz, T. Silva, A. Morillo-Candas, O. Guaitella, A. Tejero-del-Caz, L.L. Alves, V. Guerra, Influence of N_2 on the CO_2 vibrational distribution function and dissociation yield in non-equilibrium plasmas, J. Phys. D Appl. Phys. 53 (9) (2020) 094002, https://doi.org/10.1088/1361-6463/ab55fb.
[63] M. Ramakers, I. Michielsen, R. Aerts, V. Meynen, A. Bogaerts, Effect of argon or helium on the CO_2 conversion in a dielectric barrier discharge, Plasma Processes Polym. 12 (8) (2015) 755–763, https://doi.org/10.1002/ppap.201400213.
[64] J. Slaets, M. Aghaei, S. Ceulemans, S. Van Alphen, A. Bogaerts, CO_2 and CH_4 conversion in "real" gas mixtures in a gliding arc plasmatron: how do N_2 and O_2 affect the performance? Green Chem. 22 (4) (2020) 1366–1377, https://doi.org/10.1039/C9GC03743H.
[65] R. Snoeckx, K. Van Wesenbeeck, S. Lenaerts, M.S. Cha, A. Bogaerts, Suppressing the formation of NO_X and N_2O in CO_2/N_2 dielectric barrier discharge plasma by adding CH_4: scavenger chemistry at work, Sustainable Energy Fuels 3 (6) (2019) 1388–1395, https://doi.org/10.1039/C8SE00584B.
[66] P.C. Cosby, Electron-impact dissociation of nitrogen, J. Chem. Phys. 98 (12) (1993) 9544–9553, https://doi.org/10.1063/1.464385.